Eur. Phys. J. E (2011) **34**: 129
DOI 10.1140/epje/i2011-11129-1

THE EUROPEAN PHYSICAL JOURNAL E

Regular Article

Rubber friction: Comparison of theory with experiment

B. Lorenz[1,2,a], B.N.J. Persson[1,a,b], S. Dieluweit[3], and T. Tada[4]

[1] IFF, FZ-Jülich, D-52425 Jülich, Germany
[2] IFAS, RWTH Aachen University, D-52074 Aachen, Germany
[3] ICS, FZ-Jülich, D-52425 Jülich, Germany
[4] Sumitomo rubber industries, 2-1-1, Tsutsui-cho, Chuo-ku, Kobe 651-0071, Japan

Received 1 August 2011
Published online: 6 December 2011 –

Abstract. We have measured the friction force acting on a rubber block slid on a concrete surface. We used both unfilled and filled (with carbon black) styrene butadiene (SB) rubber and have varied the temperature from $-10\,^{\circ}$C to $100\,^{\circ}$C and the sliding velocity from $1\,\mu$m/s to $1000\,\mu$m/s. We find that the experimental data at different temperatures can be shifted into a smooth master-curve, using the temperature-frequency shifting factors obtained from measurements of the bulk viscoelastic modulus. The experimental data has been analyzed using a theory which takes into account the contributions to the friction from both the substrate asperity-induced viscoelastic deformations of the rubber, and from shearing the area of real contact. For filled SB rubber the frictional shear stress $\sigma_{\rm f}$ in the area of real contact results mainly from the energy dissipation at the opening crack on the exit side of the rubber-asperity contact regions. For unfilled rubber we instead attribute $\sigma_{\rm f}$ to shearing of a thin rubber smear film, which is deposited on the concrete surface during run in. We observe very different rubber wear processes for filled and unfilled SB rubber, which is consistent with the different frictional processes. Thus, the wear of filled SB rubber results in micrometer-sized rubber particles which accumulate as dry dust, which is easily removed by blowing air on the concrete surface. This wear process seams to occur at a steady rate. For unfilled rubber a smear film forms on the concrete surface, which cannot be removed even using a high-pressure air stream. In this case the wear rate appears to slow down after some run in time period.

1 Introduction

Rubber friction is a topic of huge practical importance, *e.g.*, for tires, rubber seals, wiper blades, conveyor belts and syringes [1–22]. In most practical applications, *e.g.*, for tire dynamics, rubber friction is usually described using very simple models, *e.g.*, the Coulomb friction law with a friction coefficient which may depend on the local sliding velocity and local pressure. However, this approach is purely phenomenological and cannot predict how the friction changes with the type of rubber, or with variations of the temperature or road (or substrate) roughness. In addition, rubber friction in general depends on the sliding history (memory effects) which is not included in this approach.

There are several different contributions to rubber friction as illustrated in fig. 1: (a) The substrate asperities deform the rubber which during sliding gives rise to dissipation of energy in the bulk of the rubber (pink light-dotted area) [5]. (b) Close to the opening crack tips very large viscoelastic deformations may occur resulting in a locally very large energy dissipation (pink heavy-dotted area) [23, 24]. (c) There will also be a contribution to the energy dissipation from shearing a thin contamination film (green area) on the rubber surface and/or on the substrate surface [25]. In the absence of such a film direct bonding between the rubber molecules and the substrate, followed by viscoelastic deformation and bond breaking, will also contribute to the energy dissipation and the sliding friction [11]. (d) In addition, a contribution to rubber friction will arise from wear processes, *e.g.*, the energy necessary to propagate cracks in the rubber surface region resulting in the removal of small rubber particles.

One of us has recently developed a detailed rubber friction theory involving process (a) in fig. 1 (see refs. [5, 6]). This theory is based on a new contact mechanics theory which accurately takes into account all relevant length scales [5, 26]. The theory predicts how the rubber-substrate contact area varies with the sliding velocity and the temperature, and is the basis for the study presented below. In the present analysis we also take into account processes (b) and (c). To calculate the contribution from the opening crack, we use the theory of cracks in viscoelas-

[a] www.MultiscaleConsulting.com
[b] e-mail: b.persson@fz-juelich.de

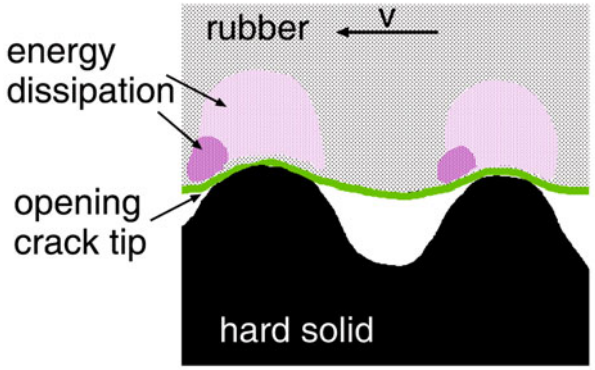

Fig. 1. (Colour on-line) Different contributions to rubber friction: (a) The substrate asperities deform the rubber which during sliding gives rise to dissipation of energy in the bulk of the rubber (pink light-dotted area). (b) Close to the opening crack tips very large viscoelastic deformations may occur resulting in a locally very large energy dissipation (pink heavy-dotted area). (c) In addition there will be a contribution to the energy dissipation from shearing a thin contamination film (green area) on the rubber surface and/or on the substrate surface. In the absence of such a film direct bonding between the rubber molecules and the substrate, followed by viscoelastic deformation and bond breaking, will also contribute to the energy dissipation and the sliding friction.

tic solids developed in [23, 27–29], where the velocity dependence of the crack propagation energy $G(v)$ can be calculated directly from the viscoelastic modulus $E(\omega)$. For process (c) we use experimental [25] and computer simulation [30] studies which show that during shearing of thin confined fluid (or soft solid) layers the shear stress $\sigma_{\rm f} \approx B\dot{\gamma}^{\alpha}$, where $\dot{\gamma}$ is the shear rate, and where B and α are (nearly) universal numbers.

For sliding velocities above $\approx 1\,$mm/s we have shown earlier [6] that the rubber friction depends on the *history* of the sliding motion (memory effects), which is crucial for an accurate description of rubber friction. For rubber sliding on a hard rough substrate, the history dependence of the friction is mainly due to frictional heating in the rubber-substrate contact regions. Many experimental observations, such as an apparent dependence of the rubber friction on the normal stress, can be attributed to the influence of frictional heating on the rubber friction. In the present study we consider only so low sliding velocities that heating effects can be neglected.

The outline of this paper is as follows: In sect. 2 we present the basic equations we use to calculate the contribution to the friction from processes (a)-(c). Section 3 describes the experimental apparatus we have developed for measuring rubber friction as a function of the sliding speed and the temperature. Section 4 presents the experimental results and the comparison with the theory prediction. In sect. 5 we discuss some aspects of the obtained results, and the relation between rubber friction and rubber wear. Section 6 contains the summary and conclusions.

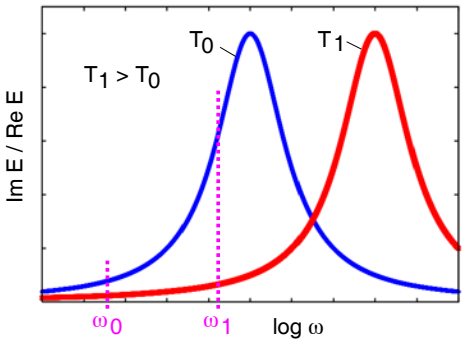

Fig. 2. When the temperature increases the $\tan\delta = \mathrm{Im}\,E/\mathrm{Re}\,E$ spectra shift to higher frequencies, which results in a decrease in the rubber friction. We assume the road asperities give rise to pulsating frequencies in the range ω_0 and ω_1.

2 Rubber friction

In this section we present the basic equations we have used to calculate the contribution to the friction from processes (a)-(c) described in the introduction. We also discuss the basic physics involved in each case.

(a) Asperity-induced bulk energy dissipation

Here we consider the energy dissipation from the viscoelastic deformations of the rubber surface by the road (or substrate) asperities. An asperity contact region with diameter d gives rise to time-dependent (pulsating) deformations of the rubber which is characterized by the frequency $\omega = v/d$, where v is the sliding velocity. The viscoelastic deformation (and most of the energy dissipation) extends into the rubber by the typical distance d. So most of the energy dissipation occurs in a volume element of order d^3. In order to have a large asperity-induced contribution to the friction, the frequency ω should be close to the maximum of the $\tan\delta = \mathrm{Im}\,E(\omega)/\mathrm{Re}\,E(\omega)$ curve. Here $\mathrm{Re}\,E(\omega)$ and $\mathrm{Im}\,E(\omega)$ are the real and imaginary part of the viscoelastic modulus $E(\omega)$ of the rubber. In reality there will be a wide distribution of asperity contact sizes, so there will be a wide range of perturbing frequencies, say from ω_0 to ω_1, see fig. 2. A large friction requires that $\tan\delta$ is as large as possible for all these perturbing frequencies.

The temperature dependence of the viscoelastic modulus of rubber-like materials is usually very strong, and an increase in the temperature by $10\,^{\circ}$C may shift the $\tan\delta$ curve to higher frequencies by one frequency decade. This will usually reduce the rubber friction, see fig. 2.

Real surfaces have a wide distribution of asperity sizes. The best picture of a rough surface is to think about it as big asperities on top of which occur smaller asperities on top of which occur even smaller asperities, ... This is illustrated in fig. 3 for a case where roughness occurs on two length scales. To get the total energy dissipation during sliding on a real surface one needs to sum up the contribution from asperity-induced deformations

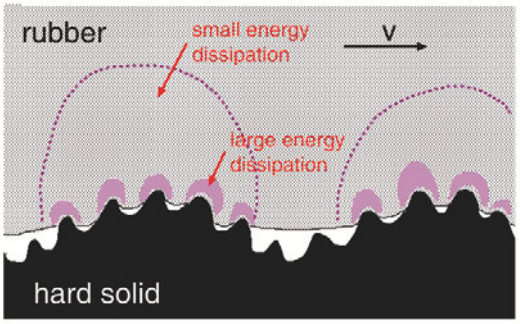

Fig. 3. The dissipated energy per unit volume is highest in the smallest asperity contact regions.

of the rubber on all (relevant) length scales. It is important to note that all length scales are *a priori* equally important [5] and a short-wavelength roughness component (wavelength λ_1, amplitude h_1) can give a contribution which is equally important as a long-wavelength roughness component (wavelength λ_0, amplitude h_0) if the ratio $h_1/\lambda_1 \approx h_0/\lambda_0$ (see ref. [5]).

Temperature has a crucial influence on rubber friction. The viscoelastic energy dissipation results in local heating of the rubber in exactly the region where the energy dissipation occurs. This results in a temperature increase, which becomes larger as we observe smaller and smaller asperity contact regions. This local (in time and space) temperature increase, resulting from the local viscoelastic energy dissipation, is referred to as the *flash temperature*. The flash temperature has an extremely important influence on the rubber friction. However, for sliding velocities $v < 1\,\mathrm{mm/s}$ the produced heat has enough time to diffuse away from the asperity contact regions, and the flash temperature effect is negligible. In the present study the friction force is measured (at different temperatures) for velocities between $1\,\mu\mathrm{m/s}$ and $1\,\mathrm{mm/s}$. Thus we can neglect frictional heating effects.

In the friction theory developed in ref. [6] only the surface roughness with wave vectors $q < q_1$ is assumed to contribute to the friction. For clean road surfaces we determine the cut-off wave vector q_1 by a yield condition: We assume that the local stress (and temperature) in the asperity contact regions on the length scale $1/q_1$ are so high that the rubber bonds break, resulting in a thin modified (dead) layer of rubber at the surface region of thickness $\approx 1/q_1$. On contaminated road surfaces, the cut-off q_1 may be determined by the nature of the contamination. The mechanism we have proposed for the determination of q_1, namely the formation of a thin modified (dead) layer at the rubber surface as a result of the high stresses and temperatures the tread rubber surface is exposed to during slip, is closely related to rubber wear. Rubber wear occurs during slip, and the track gets contaminated by small wear particles or smear which will also have some influence on the sliding friction. The cut-off length $1/q_1$ depends in general on the rubber compound used, and on the nature of the road (or substrate) surface (so changing the substrate surface requires some short run-in in order for a new thin modified surface layer to form on the tread block (corresponding to a new cut-off length)). In the study below we use $q_1 = 5 \times 10^6\,\mathrm{m}^{-1}$, which is consistent with the linear size of the (smallest) wear particles we observe, which are of order a few micrometers.

Based on the picture presented above, in ref. [6] we have derived a set of equations describing the friction acting on a rubber block squeezed with the stress σ_0 against a hard randomly rough surface. Here we summarize the basic equations. The nominal frictional stress $\sigma_{\mathrm{f0}} = \mu\sigma_0$ is determined by the following set of equations:

$$\mu \approx \frac{1}{2}\int_{q_0}^{q_1} \mathrm{d}q\, q^3 C(q) P(q) \int_0^{2\pi} \mathrm{d}\phi \cos\phi\, \mathrm{Im}\, \frac{E(qv\cos\phi)}{(1-\nu^2)\sigma_0}\,. \tag{1}$$

The function $P(q)$ is given by

$$P(q) = \frac{2}{\pi}\int_0^{\infty} \mathrm{d}x \frac{\sin x}{x} \exp[-x^2 G(q)] = \mathrm{erf}\left(\frac{1}{2\sqrt{G}}\right), \tag{2}$$

where

$$G(q) = \frac{1}{8}\int_{q_0}^{q} \mathrm{d}q\, q^3 C(q) \int_0^{2\pi} \mathrm{d}\phi \left|\frac{E(qv\cos\phi)}{(1-\nu^2)\sigma_0}\right|^2. \tag{3}$$

The normalized contact area is given by $A/A_0 = P(q_1)$.

(b) Energy dissipation at opening crack

The propagation of cracks in rubber is fundamental for many important applications, *e.g.*, rubber wear [31], for pressure sensitive adhesives [32], and also for sliding or rolling friction [24]. The strength of adhesion and cohesion of elastomers can be characterized by the amount of energy G required to advance the crack tip by one unit area. Experiments have shown that G depends on the crack tip velocity v and on the temperature T and that [33–35]

$$G(v,T) = G_0[1 + f(v,T)]. \tag{4}$$

Here we are interested in interfacial (between the rubber and the substrate) crack propagation. In this case, when viscous effects in the rubber are negligible, the measured value of G at extremely low crack velocities is of order $\approx 0.1\,\mathrm{J/m^2}$. This can be identified as G_0 and represent the energy to break the interfacial rubber-substrate bonds, which usually are of the van der Waals type. For simple hydrocarbon elastomers, the effect of temperature can be completely accounted for by applying a simple multiplying factor, denoted by a_T, to the crack velocity v, *i.e.*, $f(v,T) = f(a_T v)$. Moreover, values of a_T determined experimentally are equal to the Williams-Landel-Ferry (WLF) [36] function determined from the temperature dependence of the bulk viscoelastic modulus. This clearly proves that the large effects of crack velocity and temperature on crack propagation in rubber materials are due to viscoelastic processes in the bulk.

In (4) the function $f(v,T) = f(a_T v)$ describes the bulk viscoelastic energy dissipation in front of the crack

tip. This term is determined by the viscoelastic modulus $E(\omega)$ of the rubber, and can be calculated theoretically. The factor G_0 is due to the bond breaking (in our applications between the rubber and the substrate) at the crack tip (in the so called *crack-tip process zone*), which may involve highly non-linear processes. This term cannot be calculated theoretically, and must be deduced directly from experimental data. However, the strongest velocity dependence in (4) is derived from the factor $f(v,T)$ which may enhance G by a factor 10^3 or more at high crack tip velocities.

In refs. [23,27] we have shown that

$$G(v) = G_0 \left[1 - \frac{2}{\pi} E_0 \int_0^{2\pi v/a} \mathrm{d}\omega \frac{F(\omega)}{\omega} \,\mathrm{Im}\, \frac{1}{E(\omega)}\right]^{-1}, \quad (5)$$

where $E_0 = E(0)$ and where

$$F(\omega) = \left[1 - \left(\frac{\omega a}{2\pi v}\right)^2\right]^{1/2}. \quad (6)$$

The crack tip radius $a = a(v)$ depends on the crack tip velocity v (and temperature), and can be determined if one assumes that the stress at the crack tip takes some critical value σ_c. This gives

$$\frac{a}{a_0} = \frac{G}{G_0}, \quad (7)$$

where a_0 is the crack-tip radius for a very slowly moving crack. For high crack tip velocities $G(v) \approx G_0 E(\infty)/E(0) \gg G_0$. This is possible only if the denominator in (5) is close to zero for high crack tip velocities which means that the term involving the integral must be close to unity. If (5) is used directly to calculate $G(v)$ numerically, this requires that $E(\omega)$ is accurately known for all frequencies, which is usually not the case. However, it is possible to rewrite (5) in a form convenient for numerical calculations.

In practical applications $E(\omega)$ is known only for some finite range of frequencies $\omega_0 < \omega < \omega_1$. In order to obtain accurate results, ω_0 should be in the rubbery region so that $E(0) \approx E(\omega_0)$ and ω_1 in the glassy region so that $E(\infty) \approx E(\omega_1)$. Since the frequency range from ω_0 to ω_1 usually extends over many decades (typically 10 decades or more) it is not practical to perform the frequency integral in (5) directly, but the integral can be performed effectively if one substitutes ω with $\omega_0 e^{\xi}$. In ref. [23] we have shown that

$$\frac{a_0}{a} = 1 - \left(1 - \frac{E(\omega_0)}{E(\omega_1)}\right) \frac{\int_0^{\xi^*} \mathrm{d}\xi F(\omega_0 e^{\xi}) \,\mathrm{Im}[1/E(\omega_0 e^{\xi})]}{\int_0^{\xi^*} \mathrm{d}\xi \,\mathrm{Im}[1/E(\omega_0 e^{\xi})]}, \quad (8)$$

where

$$F(\omega_0 e^{\xi}) = \left[1 - e^{2(\xi - \xi^*)}\right]^{1/2} \quad (9)$$

and

$$\xi^* = \ln\left(\frac{2\pi v a_T}{a\omega_0}\right), \quad (10)$$

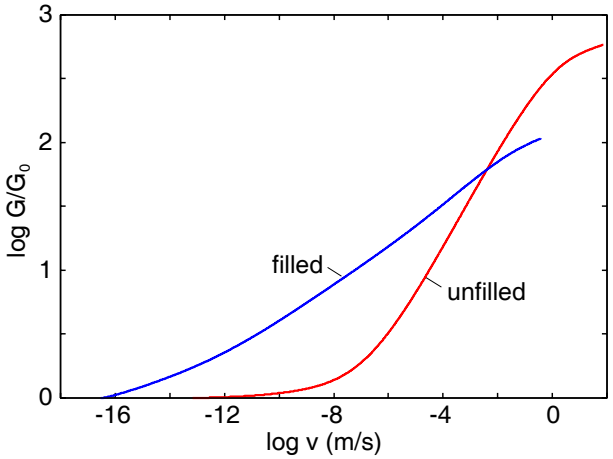

Fig. 4. The logarithm (with 10 as basis) of the crack propagation energy enhancement factor $G(v)/G_0$ as a function of the logarithm (with 10 as basis) of the crack tip velocity for filled and unfilled SB rubber.

where a_T is the temperature-frequency shifting factor. Equation (8) is easy to solve for $a(v)$ by iteration, and from the crack tip radius one can calculate $G(v) = G_0 a(v)/a_0$.

Let σ_f be the effective frictional stress acting in the area of real contact derived from the energy dissipation at the opening crack. If A is the area of real contact the energy dissipation during sliding distance $\mathrm{d}x$ is

$$\sigma_f A \mathrm{d}x = G(v) N l \mathrm{d}x. \quad (11)$$

Here we have assumed that the contact area consists of N regions of linear size l. Thus $Nl\mathrm{d}x$ is the surface area covered by the crack during the sliding distance $\mathrm{d}x$. Since $A = Nl^2$, we get

$$\sigma_f = G(v)/l. \quad (12)$$

Real rubber materials, in particular filled rubbers, exhibit non-linear rheological properties, and the viscoelastic modulus $E(\omega)$, which enters both in the crack propagation theory and in the theory of friction presented in point (a) of sect. 2, should be measured at as large strain (or stress) as possible because the strain (or stress) in the vicinity of a crack tip, or at an asperity contact region, will in general be very high.

In fig. 4 we show the interfacial crack propagation energy enhancement factor $G(v)/G_0$, as a function of the logarithm of the crack tip velocity v for filled and unfilled SB rubber. This function is calculated using (8)-(10) with $a_0 = 1\,\mathrm{nm}$.

(c) Energy dissipation in shearing a thin viscous film

Many fluids, in particular polymer fluids, *e.g.*, high viscosity silicon oils, undergo shear thinning at relative low shear rate. The viscosity is often well approximated by

$$\eta(u,v) \approx \frac{\eta_0}{1 + (\eta_0/B)\dot{\gamma}^n}, \quad (13)$$

where η_0 is the viscosity at low shear rate, and where the shear rate $\dot{\gamma} = v/u$ (where u is the film thickness). At

low shear rate, where the fluid viscosity is constant, the orientations of the fluid molecules are random. Shear thinning involves orientation of the molecules along the flow direction. A similar effect as shear thinning is the effect of confinement of the molecules between closely spaced solid walls, where the molecules tend to form layers parallel to the solid walls. Equation (13) is also valid for nanometer-thick confined layer but in this case the shear rate is always so large that (13) takes the form

$$\eta(u,v) \approx B\dot{\gamma}^{-n}, \tag{14}$$

giving the shear stress

$$\sigma_{\rm f} = \eta\dot{\gamma} \approx B\dot{\gamma}^{\alpha}, \tag{15}$$

where the exponent $\alpha = 1 - n$ is $\alpha \approx 0.1$ [25]. If $\sigma_{\rm f}$ is in units of Pa s and $\dot{\gamma}$ in units of $\rm s^{-1}$, then $B \approx 8.0 \times 10^4$ [25]. We note that confined layers often are better characterized as soft solids even if the confined material is a fluid when confined between solids walls at large (macroscopic) separation.

3 Experimental

We have developed a new instrument, shown schematically in fig. 5, in order to test the rubber friction theory presented above. A rubber block is attached to the lower surface of an aluminum plate and brought into contact with a randomly rough substrate. The nominal force $F_{\rm N}$ can be changed by adding plates with different weights on top of the aluminum plate. The rough surface is clamped to a steel sledge which is moved using a voice coil actuator. This actuator is capable to generate a constant force without force ripples, leading to a constant velocity even at very low velocities. The position of the sledge is measured to control the actuator and its velocity. In order to avoid flash temperature effects, the sliding velocities are small. The highest possible velocity was of order 1 mm/s while the lowest velocity used was 0.5 μm/s. To control the velocity, the position of the sledge is gauged using an analog magnetostrictive position encoder with an absolute resolution of $< 10\,\mu$m. The stroke of the sledge is 50 mm.

The friction force is measured using a tension and compression load cell that is mounted in line with the rubber-substrate interface to avoid torque. The friction forces in the linear ball bearing system are excluded from the results of the force measurements. The force cell can be replaced in order to change the effective range of the sensor. The resolution depends on the load cell used, but is always of order 0.2 N or better. The experimental set-up is placed inside a temperature box where the temperature can be changed from $-10\,^{\circ}$C to above 120 °C. The heating is built in the upper aluminum plate as well as in the ground plate of the linear guides to ensure a homogeneous temperature distribution.

The experiment is performed as follows. A rubber test specimen is cut out off a rubber sheet and then clamped onto a sample holder. The rubber usually has a surface

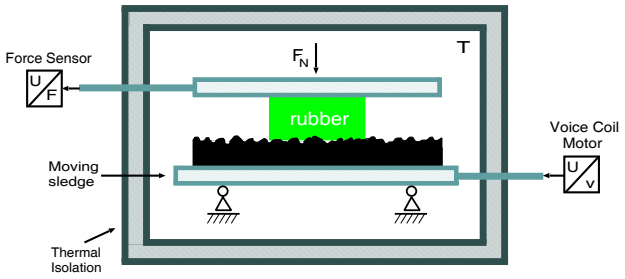

Fig. 5. A rubber block is squeezed against a rough substrate. The substrate is clamped on a sledge that is moved with a constant velocity v. The friction force of the rubber is measured using a load cell. The set-up is located inside a box where the temperature T can be changed from $-10\,^{\circ}$C to $> 120\,^{\circ}$C. The friction forces are measured at different velocities and temperatures and then shifted according to the WLF equation to a master curve.

layer with different properties from its bulk material resulting from the production process and/or because of storing it for a long time. This layer is removed by wearing the rubber surface with sandpaper with small grain sizes. The specimen with the sample holder is then placed in the instrument, brought into contact with the rough counter surface and a constant nominal force is applied. The sample is run-in at room temperature, with a sliding velocity of about 1 mm/s, until the friction force reaches a steady-state condition. Depending on the rubber material, the run-in time needed can vary quite strongly. It is proposed to run-in the specimen at high sliding velocities because of the modified layer the rubber develops at the interface. In order to have the same properties for the rubber during the whole experiment, the thickness of this layer should be large so that even if rubber particles are removed from the interface, *e.g.* because of wear, one has still the same layer with equal properties for the whole study.

After this preparation procedure the sliding velocity is varied from high to low velocities and the friction force is measured. For each velocity, the rubber sample is slid in an oscillatory manner until a stable friction value could be measured. When the experiment is completed for all the necessary velocities, the temperature T is changed and the whole procedure is repeated. Finally, the experiment is repeated at room temperature to crosscheck the results obtained in the beginning. The different curves are then shifted to a master curve using the same shifting factors a_T as resulted from the measurement of the viscoelastic modulus.

The surface roughness of the concrete surface used in this experiment was measured using different methods, namely 1D stylus linescan, 2D optical data using a white light interferometry sensor and an infinite focus microscope, as well as atomic force microscopy (AFM). The surface roughness power spectra were calculated using all these pieces of information about the surface height profile, see fig. 6. The power spectra obtained from the data of the stylus line scan joins with the power spectra of the AFM measurements in the overlapping wave vector range. The power spectra from the optical measurements

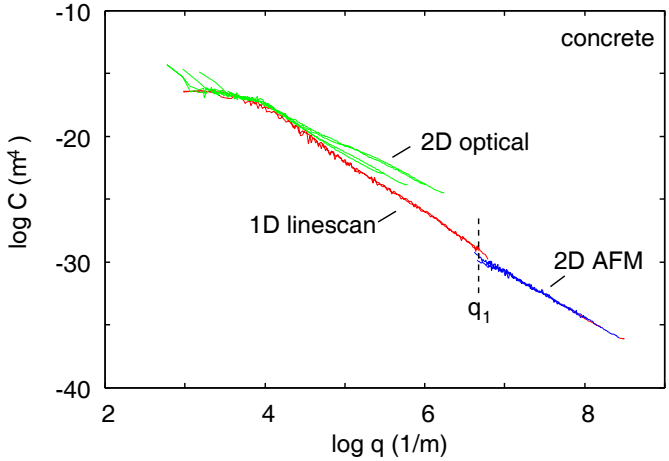

Fig. 6. (Colour on-line) The logarithm (with 10 as basis) of the surface roughness power spectrum, $C(q)$, as a function of the logarithm (with 10 as basis) of the wave vector q, for the concrete surface used in the sliding friction experiments. The power spectrum was obtained from stylus line scan data (red line) and optical 2D measurements (green line) for small wave vectors, and from AFM data (blue line) for large wave vectors. The large wave vector cut-off, q_1, used in the calculations of the asperity-induced viscoelastic contribution to the rubber friction, is indicated.

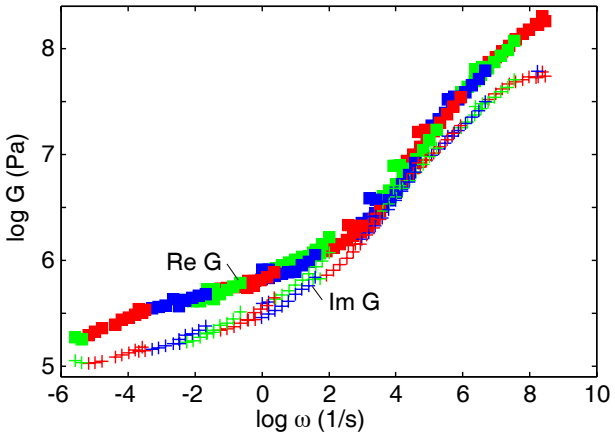

Fig. 7. (Colour on-line) The logarithm (with 10 as basis) of the real and imaginary part of the shear modulus G as a function of the logarithm of the frequency ω for the unfilled rubber used in the rubber friction experiments. The modulus was measured at constant stress amplitude and at several different temperatures and shifted to obtain the master curve at $T = 27\,^{\circ}\mathrm{C}$. The measurements were performed at (from low to high frequency) 80, 60, 50, 40, 30, 20, 10, 0, −10, −15, −20, −25, and −30 °C.

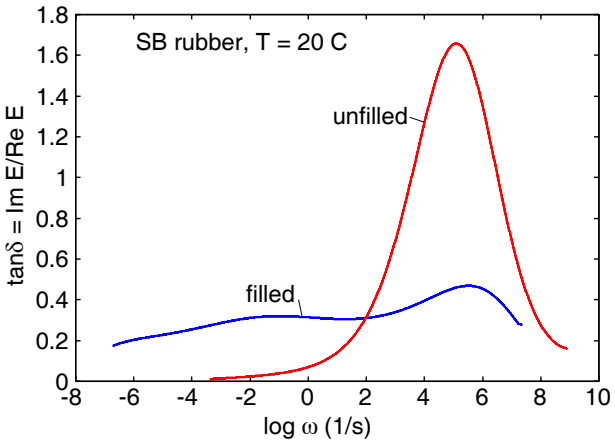

Fig. 8. The $\tan\delta(\omega) = \mathrm{Im}\,E(\omega)/\,\mathrm{Re}\,E(\omega)$ as a function of the logarithm (with 10 as basis) of the frequency ω for the filled and unfilled rubber used in the rubber friction experiments. The modulus was measured at constant stress amplitude.

obtained using two different sensors deviate at small wave vectors. In the calculations used below, only the power spectra from the line scan and the AFM data is used. Also indicated in this figure is the large cut-off wave vector q_1 used in the analysis.

The viscoelastic modulus of the rubbers used is studied using dynamic mechanical analysis (DMA). The shear modulus $G(\omega)$ is measured in oscillatory shear mode at a constant force amplitude of 25 N corresponding to a stress amplitude of ≈ 0.25 MPa. The rubber sample is fixed at both interfaces and then sheared at different frequencies. To obtain a broad master curve, this is repeated at several different temperatures. The data is then shifted along the frequency axis, similar to the friction results for different temperatures, and the shift factors a_T are obtained. No vertical shifting was performed. In fig. 7 we show the logarithm (with 10 as basis) of the real and imaginary part of the shear modulus G as a function of the logarithm of the frequency ω for the unfilled rubber used in the rubber friction experiments. $G(\omega)$ is measured at several different temperatures and shifted to obtain the master curve at $T = 27\,^{\circ}\mathrm{C}$. The measurements were performed at (from low to high frequency) 80, 60, 50, 40, 30, 20, 10, 0, −10, −15, −20, −25, and −30 °C and different temperature segments of the $G(\omega)$-curve are denoted by green, red, blue, green, ...

In fig. 8 the $\tan\delta = \mathrm{Im}\,E(\omega)/\,\mathrm{Re}\,E(\omega)$ curve is shown as a function of the logarithm of the frequency for both rubber samples.

An important issue for measuring the viscoelastic modulus of real rubber materials, in particular filled rubber, is that they exhibit non-linear rheological properties. As $E(\omega)$ enters in both dissipation mechanisms (a) and (b), how this quantity is measured is of great importance. Because of the very high strain (or stress) in the asperity contact regions as well as in the vicinity of a crack tip, it is suggested to measure at as large strain (or stress) as possible to account for these non-linear properties, *e.g.* Paine effect or Mullins effect.

4 Experimental results and analysis

We first present and analyze the results for unfilled SB rubber and then for filled SB rubber. In all cases the rubber block is slid on the concrete surface with the surface roughness power spectrum shown in fig. 6. The surface roughness on the rubber tread block is neglected in the analysis presented below.

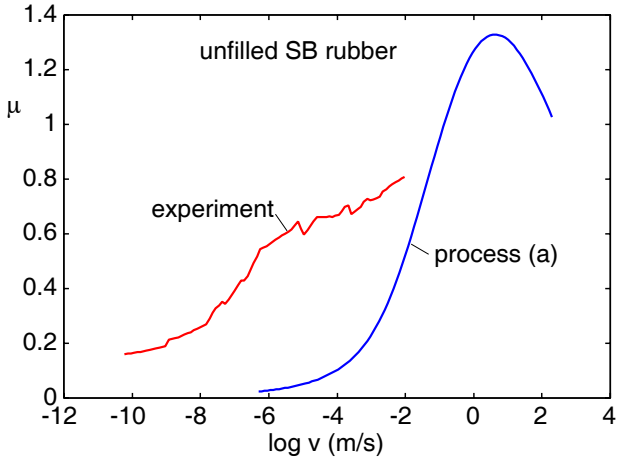

Fig. 9. (Colour on-line) The measured friction coefficient as a function of the logarithm (with 10 as basis) of the sliding velocity. Also shown (blue curve) is the calculated friction coefficient accounting only for the asperity-induced viscoelastic contribution to the rubber friction (process (a)).

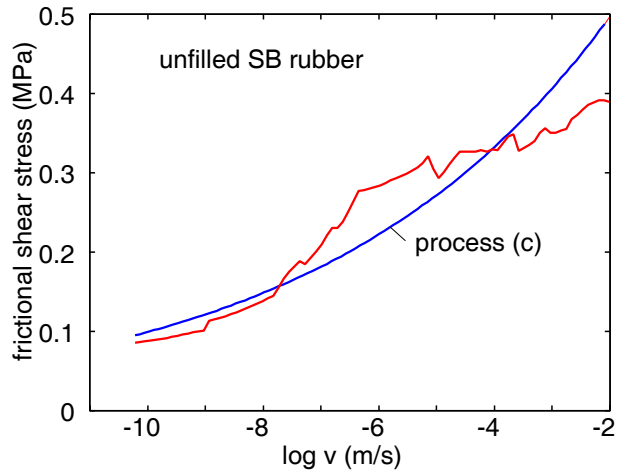

Fig. 10. (Colour on-line) The calculated frictional shear stress acting in the area of real contact as a function of the logarithm (with 10 as basis) of the sliding velocity. The blue line is a fit to the frictional shear stress assuming $\sigma_f = Cv^\alpha$ with (in SI units) $C = 7.45 \times 10^5$ and $\alpha = 0.0875$ (process (c)).

4.1 Unfilled SB rubber

Figure 9 shows the measured friction coefficient (red curve) as a function of the logarithm of the sliding velocity. Also shown (blue curve) is the calculated friction coefficient accounting only for the asperity-induced viscoelastic contribution (process (a)) to the rubber friction. For sliding velocities $v < 0.1$ mm/s, the contribution from process (a) to the total friction is negligible, while it dominates for $v > 10$ mm/s. We now show that for $v < 1$ mm/s the main contribution to the friction is associated with shearing a thin confined contamination (or smear) film in the asperity contact regions.

Figure 10 shows the frictional shear stress σ_f acting in the area of real contact as a function of the logarithm of the sliding velocity. The red line has been deduced from the measured friction using $[\mu(\text{exp}) - \mu(\text{process(a)})]\sigma_0 A_0/A$, where A is the area of real contact and $\sigma_0 = 0.065$ MPa the nominal squeezing pressure. The blue line is the predicted frictional shear stress $\sigma_f = Cv^\alpha$ where (in SI units) $C = 7.45 \times 10^5$ and $\alpha = 0.0875$. If we assume that the region undergoing shear is of order $d = 3$ nm thick [37] then since the shear rate $\dot\gamma = v/d$ we get $\sigma_f = B\dot\gamma^\alpha$ with (in SI units) $B = Cd^\alpha \approx 1.34 \times 10^5$. Thus the frictional shear stress is rather well described by eq. (15) with parameters B and α in close agreement with values deduced from direct measurements [25] (and molecular dynamics calculations [30]) of confined hydrocarbon films. This is a strong indication that in this case σ_f originates from shearing a thin confined contamination (or smear) film.

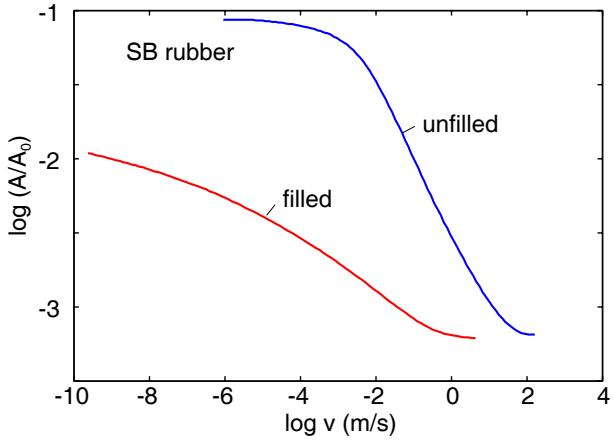

Fig. 11. The relative area of real contact for the filled and unfilled SB rubber as a function of the logarithm of the sliding velocity.

Note that for $v > 1$ mm/s the contribution to the friction from shearing the contamination film rapidly decreases with increasing velocity, as a result of the decrease in the area of real contact. Thus, fig. 11 shows the relative area of real contact for the unfilled (and filled) SB rubber as a function of the logarithm of the sliding velocity. At low sliding velocities the area of real contact is nearly 10% of the nominal contact area, but at high velocities, where the rubber appears stiff, only 0.1% of the nominal contact area. There is no reason why the frictional shear stress from shearing the contamination film will exhibit the same temperature dependence as the bulk viscoelastic contribution, but rather σ_f is expected to exhibit a rather weak temperature dependence. The fact that the friction coefficient nevertheless (approximately) obeys the WLF-type of temperature-velocity shifting is due to fact that the area of real contact exhibits the WLF shifting. At high velocity the contact area becomes small resulting in high contact pressures, *e.g.*, ≈ 10 MPa at $v = 0.1$ m/s. Molecular Dynamics simulation [38] studies have shown that the frictional shear stress due to process (c) is independent of the pressure up to ~ 30 MPa so we may still consider σ_f as pressure independent.

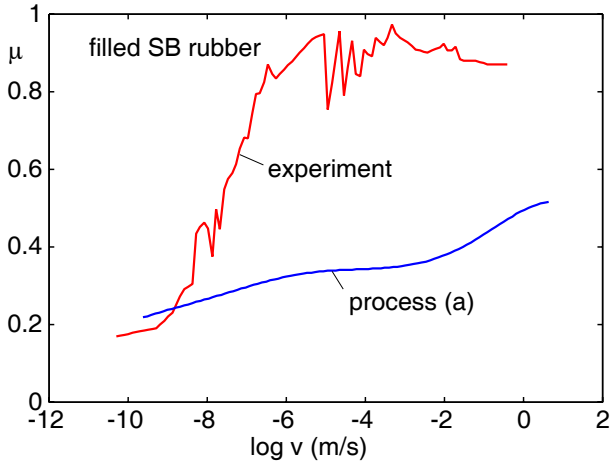

Fig. 12. (Colour on-line) The measured friction coefficient as a function of the logarithm (with 10 as basis) of the sliding velocity. Also shown (blue curve) is the calculated friction coefficient accounting only for the asperity-induced viscoelastic contribution to the rubber friction (process (a)).

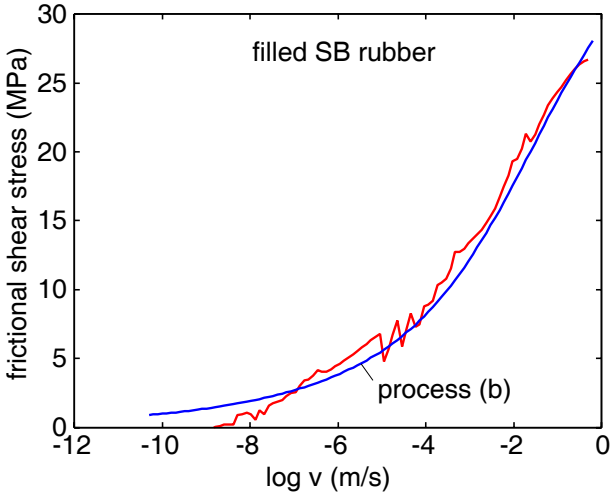

Fig. 13. (Colour on-line) The calculated frictional shear stress acting in the area of real contact as a function of the logarithm (with 10 as basis) of the sliding velocity. The blue line is a fit to the frictional shear stress assuming $\sigma_{\rm f} = \sigma_1 G(v)/G_0$ with $\sigma_1 = 0.25\,{\rm MPa}$ and $G(v)/G_0$ the viscoelastic crack propagation factor for filled SB rubber (process (b)).

4.2 Filled SB rubber

Figure 12 shows the measured friction coefficient (red curve) as a function of the logarithm (with 10 as basis) of the sliding velocity. Also shown (blue curve) is the calculated friction coefficient accounting only for the asperity-induced viscoelastic contribution (process (a)) to the rubber friction. In this case the main part of the difference between the measured friction and the contribution from process (a) cannot be explained as resulting of shearing of a thin contamination layer since the area of real contact at low sliding velocity is ~ 10 (or more) times smaller for filled SB rubber, as compared to unfilled compound, see fig. 11. Here we will instead show that the shear stress for filled SB rubber is mainly associated with the opening crack at the exit side of the asperity contact regions.

Figure 13 shows the frictional shear stress $\sigma_{\rm f}$ acting in the area of real contact as a function of the logarithm of the sliding velocity. The red line has been deduced from the measured friction using $[\mu({\rm exp}) - \mu({\rm process(a)})]\sigma_0 A_0/A$, where A is the area of real contact and $\sigma_0 = 0.065\,{\rm MPa}$ the nominal squeezing pressure. The blue line is the predicted frictional shear stress from the crack opening mechanism calculated using $\sigma_{\rm f} = G(v)/l = [G(v)/G_0][G_0/l]$ (see (12)) where $G(v)/G_0$ has been obtained using the crack propagation theory (blue line in fig. 10) and with $G_0/l = 0.25\,{\rm MPa}$. Using $G_0 = 0.1\,{\rm J/m^2}$ this implies $l = 0.4\,\mu{\rm m}$, *i.e.*, of order $\lambda_1 = 2\pi/q_1$ as expected. Note that the stress in fig. 13 is ~ 30 times bigger than would result from process (c) (compare with fig. 10) so this process gives a negligible contribution in the present case.

To check the pictures presented above, we have, performed an additional experiment with lubricated surfaces. If the lubricant film is very thin it will not affect the contribution to the friction from process (a) but it may remove (or reduce) the opening-crack contribution to the rubber friction. In the experiment a very thin film of a high viscosity ($\eta = 1\,{\rm Pa\,s}$) silicon oil was deposited uniformly on the rubber surface. This leads to a drastic reduction in the sliding friction, from $\mu \approx 0.95$ to $\mu \approx 0.34$ as shown in fig. 14. This figure shows the friction coefficient $\mu = F_x/F_z$ as a function of time at the sliding velocity $v = 50\,\mu{\rm m/s}$. At $t \approx 5000\,{\rm s}$ the oil is deposited on the rubber surface. The drop in the friction coefficient from ≈ 0.95 to ≈ 0.34 is consistent with fig. 12 (at $v = 0.005\,{\rm cm/s}$), assuming that the oil film removes the crack-opening contribution while the contribution from the asperity-induced viscoelastic deformations (process (a)) remains unchanged. The latter assumption requires that the oil film is so thin as to not modify the relevant surface roughness components on the

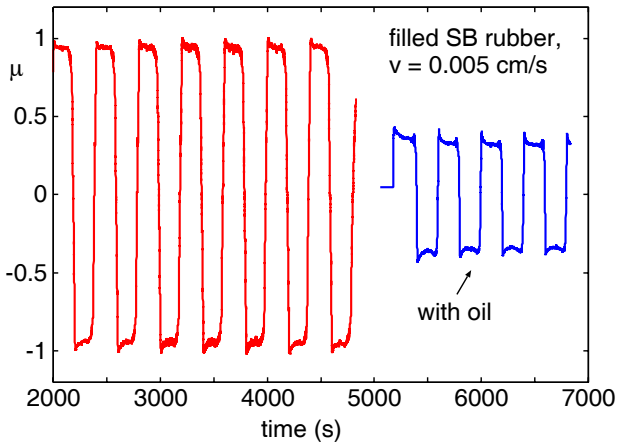

Fig. 14. The friction coefficient $\mu = F_x/F_z$ as a function of time at the sliding velocity $v = 0.005\,{\rm cm/s}$. At $t \approx 5000\,{\rm s}$ a very thin film of silicon oil is deposited on the rubber surface. This results in a drop in the friction coefficient from ≈ 0.95 to ≈ 0.34.

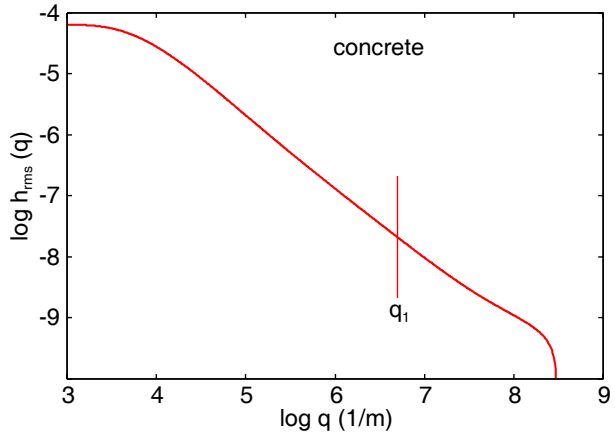

Fig. 15. The logarithm (with 10 as basis) of the root-mean-square roughness, $h_{\rm rms}(q)$, as a function of the logarithm (with 10 as basis) of the largest roughness wave vector q. In calculating $h_{\rm rms}(q)$ only roughness components with wave vector larger than q are included, *i.e.*, $h_{\rm rms}(q)$ is the root-mean-square roughness when the surface is studied over a region with linear size $\approx 2\pi/q$.

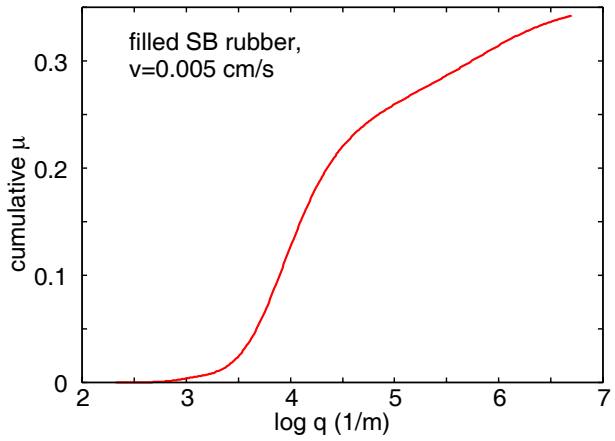

Fig. 16. The cumulative friction coefficient (from process (a)) as a function of the logarithm (with 10 as basis) of the largest roughness wave vector q included in the calculation of μ, at the sliding velocity $v = 0.005\,{\rm cm/s}$.

surface. To understand how thick the fluid film can be without affecting the friction process (a), in fig. 15 we show the logarithm of the root-mean-square roughness, $h_{\rm rms}(q)$, as a function of the logarithm of the largest roughness wave vector q. In calculating $h_{\rm rms}(q)$ only roughness components with wave vector larger than q are included, *i.e.*, $h_{\rm rms}(q)$ is the root-mean-square roughness when the surface is studied over a region with linear size $\approx 2\pi/q$. Figure 15 shows that the fluid film must be at most $\approx 10\,{\rm nm}$ in order not to reduce the contribution from process (a) to the friction. However, it turns out that the most important contribution to the friction from process (a) is derived from the surface roughness components with wave vector $q < 10^5\,{\rm m}^{-1}$ (see below), and fig. 15 shows that in order for this surface roughness region to be unaffected, it is enough that the fluid film thickness is below $\approx 1\,\mu{\rm m}$.

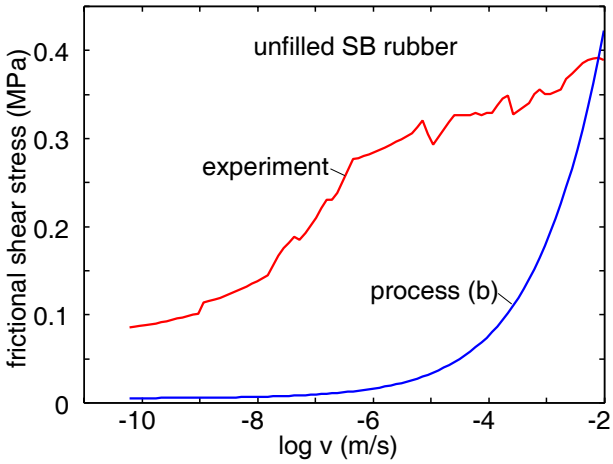

Fig. 17. (Colour on-line) The calculated frictional shear stress acting in the area of real contact as a function of the logarithm (with 10 as basis) of the sliding velocity. The blue line is a fit to the frictional shear stress assuming $\sigma_{\rm f} = \sigma_1 G(v)/G_0$, with $\sigma_1 = 5\,{\rm kPa}$ and $G(v)/G_0$ the viscoelastic crack propagation factor for unfilled SB rubber (process (b)).

Figure 16 shows the cumulative friction coefficient (at the sliding velocity $v = 0.005\,{\rm cm/s}$) associated with process (a), as a function of the logarithm of the largest roughness wave vector q included in the calculation of μ. Note that even if the lubricant film removed the last decade of surface roughness components, the friction would not drop by more then $\sim 10\%$ and including wave vectors $q < 10^5\,{\rm m}^{-1}$ still results in a friction only $\approx 20\%$ smaller that when the whole range of wave vector up to $q_1 = 5 \times 10^6\,{\rm m}^{-1}$ is included in the analysis.

5 Discussion

We have shown above that shearing a thin confined film (process (c)) cannot explain the observed shear stress $\sigma_{\rm f}$ in the area of real contact for filled SB rubber because of the small area of real contact. Although this mechanism will contribute to the observed $\sigma_{\rm f}$, the largest contribution was attributed to a crack-opening mechanism at the exit of the asperity-rubber contact regions.

However, for unfilled rubber the contribution from process (c) alone can explain the observed shear stress. Here we discuss why there might be no or negligible contribution from the crack-opening mechanism for unfilled SB rubber. Let us first show that the crack-opening mechanism would predict a much stronger dependence of $\sigma_{\rm f}$ on the velocity than observed. Thus, in fig. 17 we show the observed $\sigma_{\rm f}$ (red line) and the calculated frictional shear stress from process (b), as a function of the logarithm of the sliding velocity. The blue line is the frictional shear stress assuming $\sigma_{\rm f} = \sigma_1 G(v)/G_0$ with $\sigma_1 = 5\,{\rm kPa}$ and $G(v)/G_0$ the viscoelastic crack propagation factor for unfilled SB rubber. Obviously, the process (b) predicts a much stronger velocity dependence than observed.

We believe that the absence of the crack-opening mechanism for the unfilled rubber is related to a thin high-

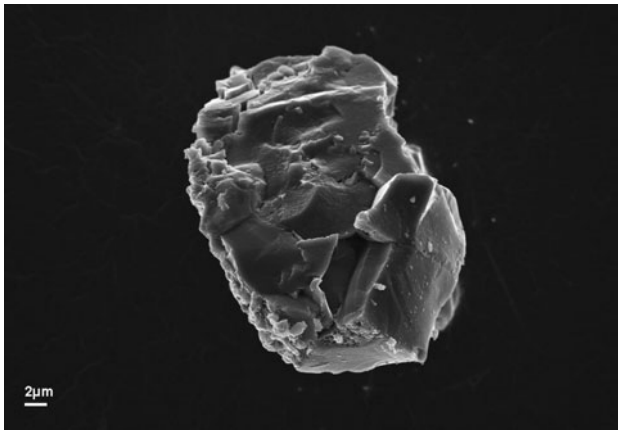

Fig. 18. Scanning electron microscopy picture of a compact rubber wear particle with diameter $\approx 20\,\mu$m.

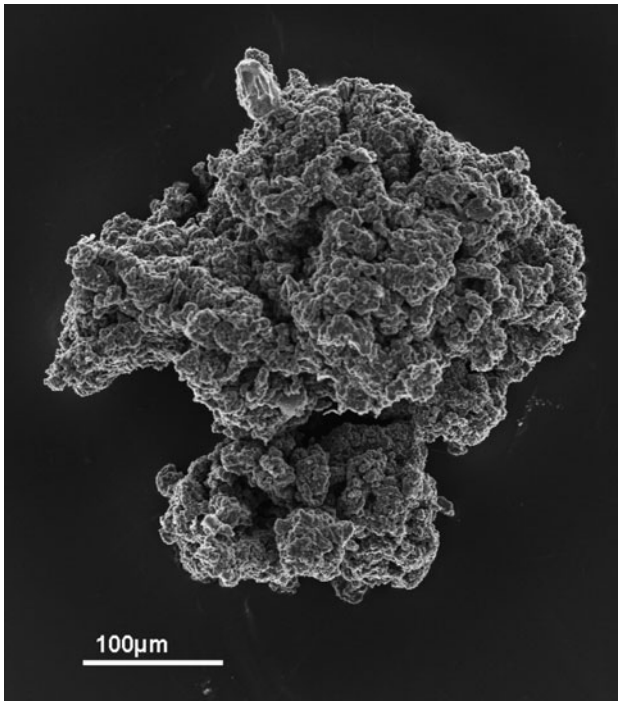

Fig. 19. Scanning electron microscopy picture of another big rubber wear particle (diameter $\approx 300\,\mu$m) consisting of an agglomerate of many small particles.

viscosity liquid-like film on the rubber and concrete surface after run-in. As pointed out before, for the unfilled SB rubber we observe a smear film on the concrete surface while for the filled rubber we observe dry dust particles (see figs. 18, 19, and 20), which are easily removed by an air stream. Consistent with this explanation is the observation that a very thin high-viscosity silicon oil film on the surface of the filled SB rubber removes the crack-opening contribution. The microscopic origin of this effect may be that with the fluid film between the surfaces the adhesional interaction is strongly reduced and there could even be an effective short-ranged repulsion between the surfaces depending on the magnitude of the relevant interfacial energies. The latter is probably the case when water containing a soap is used as "lubricant", as this fluid seems to remove the crack opening mechanism too (see ref. [39]).

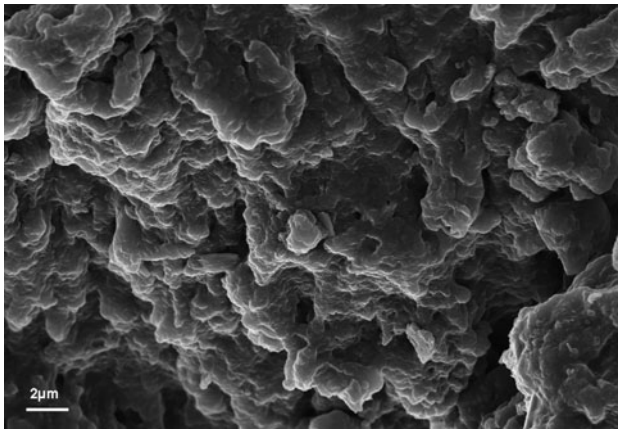

Fig. 20. Zoom-in on the wear particle in fig. 19 (about $30\,\mu\text{m} \times 20\,\mu$m surface area). Note the strong variation of the surface topography on the length scale of $\sim 1\,\mu$m.

In this paper we have proposed that for the filled rubber an important contribution to the friction force comes from adhesive interfacial crack-opening. However, an alternative explanation is that the rubber wear process itself gives an important contribution to the observed friction. But in this case, in order to explain the observed velocity dependence, one must postulate that the wear involves crack propagation with a velocity proportional to the sliding velocity, at least for high velocity or (equivalently) low temperatures. This explanation seems unlikely to us but more studies are necessary to determine the contribution to the friction from the rubber wear process (which involves removal of rubber particles by crack propagation).

Recently the contact between a rubber sphere with surface roughness and a flat glass substrate has been studied using an optical microscope. For non-lubricated rubber the area of real contact was found to increase with the sliding velocity as expected from the increase in $G(v)$ with sliding velocity [40]. In another experiment where the rubber surface was coated by a thin layer (about $0.1\,\mu$m) of silicon oil the contact area was instead found to decrease with increasing sliding velocity [41]. A decrease in the area of real contact has also been observed for silicon rubber balls sliding on (passivated) silicon wafer surfaces [42]. Fully cross-linked silicon rubber is nearly a perfect elastic solid at low frequencies, and one expects the $G(v)$ function to be large only for very large velocities. Nevertheless, it is not clear what is the origin of the decrease in the contact area in this case (see ref. [43]).

6 Summary and conclusion

We have presented a combined theoretical-experimental study of rubber friction on randomly rough surfaces. The different energy dissipation processes resulting from

asperity-induced viscoelastic bulk deformation, opening cracks and shearing a thin viscous film at the interface were discussed. We have shown results from friction experiments where a rubber block is sliding on a rough substrate with a constant velocity at different temperatures. The experimental results were compared to the theory predictions, and good agreement between theory and experiment was found.

After we had completed the study presented above, a related paper was published by Busse, Boubakri and Küppel (ref. [39]). They performed a similar experimental study as reported in our paper, but using other types of rubber and substrate surfaces. They only studied filled rubbers, but for this case they arrived at a similar conclusion as in our paper, namely that the total friction has contributions from the processes (a) and (b) discussed above.

We thank M. Klüppel for the unfilled and filled SB rubber samples. This work, as part of the European Science Foundation EUROCORES Program FANAS, was supported from funds by the DFG and the EC Sixth Framework Program, under contract N ERAS-CT-2003-980409.

References

1. B.N.J. Persson, *Sliding Friction: Physical Principles and Applications*, 2nd edition (Springer, Heidelberg, 2000).
2. K.A. Grosch, Proc. R. Soc. London, Ser. A **274**, 21 (1963).
3. A.N. Gent, J.D. Walter (Editors), *The Pneumatic Tire* (US Department of Transportation, 2006).
4. H.B. Pacejka, *Tyre and Vehicle Dynamics*, 2nd edition (Elsevier, Amsterdam, 2006).
5. B.N.J. Persson, J. Chem. Phys. **115**, 3840 (2001).
6. B.N.J. Persson, J. Phys.: Condens. Matter **18**, 7789 (2006).
7. G. Heinrich, M. Klüppel, T.A. Vilgis, Comput. Theor. Polym. Sci. **10**, 53 (2000).
8. G. Heinrich, M. Klüppel, Wear **265**, 1052 (2008).
9. M. Klüppel, G. Heinrich, Rubber Chem. Technol. **73**, 578 (2000).
10. S. Westermann, F. Petry, R. Boes, G. Thielen, Kautsch. Gummi Kunstst. **57**, 645 (2004).
11. B.N.J. Persson, A.I. Volokitin, Eur. Phys. J. E **21**, 69 (2006).
12. G. Carbone, B. Lorenz, B.N.J. Persson, A. Wohlers, Eur. Phys. J. E **29**, 275 (2009).
13. B.N.J. Persson, Surf. Sci. **401**, 445 (1998).
14. A. Le Gal, M. Klüppel, J. Chem. Phys. **123**, 014704 (2005).
15. B.N.J. Persson, J. Phys.: Condens. Matter **21**, 485001 (2009).
16. M. Mofidi, B. Prakash, B.N.J. Persson, O. Albohr, J. Phys.: Condens. Matter **20**, 085223 (2008).
17. See, *e.g.*, B.N.J. Persson, O. Albohr, U. Tartaglino, A.I. Volokitin, E. Tosatti, J. Phys.: Condens. Matter **17**, R1 (2005).
18. B.N.J. Persson, O. Albohr, C. Creton, V. Peveri, J. Chem. Phys. **120**, 8779 (2004).
19. B.N.J. Persson, J. Phys.: Condens. Matter **23**, 015003 (2011).
20. B.N.J. Persson, Eur. Phys. J. E **33**, 327 (2010).
21. D.T. Nguyen, P. Paolino, M.C. Audry, A. Chateauminois, C. Fretigny, Y.L. Chenadec, M. Portigliatti, E. Barthel, J. Adhes. **87**, 235 (2011).
22. A. Le Gal, M. Klüppel, J. Phys.: Condens. Matter **20**, 015007 (2008).
23. B.N.J. Persson, O. Albohr, G. Heinrich, H. Ueba, J. Phys.: Condens. Matter **17**, R1071 (2005).
24. G. Carbone, L. Mangialardi, J. Mech. Phys. Solids **52**, 1267 (2004).
25. S. Yamada, Tribol. Lett. **13**, 167 (2002).
26. B.N.J. Persson, Surf. Sci. Rep. **61**, 201 (2006).
27. B.N.J. Persson, E.A. Brener, Phys. Rev. E **71**, 036123 (2005).
28. G. Carbone, B.N.J. Persson, Phys. Rev. Lett. **95**, 114301 (2005).
29. G. Carbone, B.N.J. Persson, Eur. Phys. J. E **17**, 261 (2005).
30. I. Sivebaek, V. Samoilov, B.N.J. Persson, to be published.
31. G. Heinrich, J. Stuve, G. Gerber, Polymer **43**, 395 (2002).
32. C. Creton, H. Lakrout, J. Polym. Sci. B, Polym. Phys. **38**, 965 (2000).
33. A.N. Gent, J. Schultz, J. Adhesion **3**, 281 (1972).
34. D. Maugis, M. Barquins, J. Phys. D **11**, 1989 (1978).
35. A.N. Gent, Langmuir **12**, 4492 (1996).
36. M.L. Williams, R.F. Landel, J.D. Ferry, J. Am. Chem. Soc. **77**, 3701 (1955).
37. Yew *et al.* (Y.K. Yew, M. Minn, S.K. Sinha, V.B.C. Tan, Langmuir **27**, 5891 (2011)) have shown that when sliding polymer-on-polymer systems, the shear deformation is localized to a band about 3 nm thick at the interface of the polymer surfaces.
38. I. Sivebaek, V. Samolilov, B.N.J. Persson, Eur. Phys. J E **27**, 37 (2008).
39. L. Busse, I. Boubakri, M. Klüppel, Kautsch. Gummi Kunstst., May 2011, p. 35.
40. B.A. Krick, J.R. Vail, B.N.J. Persson, W.G. Sawyer, Tribology Lett., DOI: 10.1007/s11249-011-9870-y.
41. B.A. Krick, J.R. Vail, W.G. Sawyer, private communication.
42. K. Vorvolakos, M.K. Chaudhury, Langmuir **19**, 6778 (2003).
43. B.N.J. Persson, I.M. Sivebaek, V.N. Samoilov, K. Zhao, A.I. Volokitin, Z. Zhang, J. Phys.: Condens. Matter **20**, 395006 (2008).